Analytical investigation on moment-rotation relationship of through-tenon joints with looseness in ancient timber buildings

Jianyang Xue[*1], Liangjie Qi[1,2], Jinshuang Dong[1] and Dan Xu[1]

[1]*Department of Civil Engineering, Xi'an University of Architecture and Technology, Xi'an 710055, China*
[2]*Department of Civil and Environmental Engineering, Virginia Tech, Blacksburg, 24060, USA*

Abstract. To study the mechanical properties of joints in ancient timber buildings in depth, the force mechanism of the through-tenon joints was analyzed, also the theoretical formulas of the moment-rotation angles of the joints with different loosening degrees were deduced. To validate the rationality of the theoretical calculation formulas, six joint models with 1/3.2 scale ratio, including one intact joint and five loosening joints, were fabricated and tested under cyclic loading. The specimens underwent the elastic stage, the plastic stage and the destructive stage, respectively. At the same time, the moment-rotation backbone curves of the tenon joints with different looseness were obtained, and the theoretical calculation results were validated when compared with the experimental results. The results show that the rotational moment and the initial rotational stiffness of the tenon joints increase gradually with the increase of the friction coefficient. The increase of the tenon section height can effectively improve the bearing capacity of the through-tenon joints. As the friction coefficient of the wood and the insertion length of the tension increase, the embedment length goes up, whereas it decreases with the increase of section height. With the increase of the looseness, the bearing capacity of the joint is reduced gradually.

Keywords: ancient timber buildings; through-tenon joints; looseness; seismic performance; low cyclic reversed loading tests; moment-rotation relationship
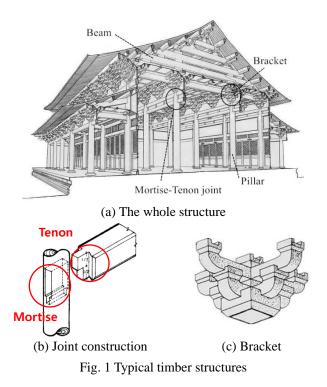
1. Introduction

Chinese ancient timber architecture is famous for its long history and unique style. One of the main features of Chinese ancient timber building is utilizing mortise-tenon joints to connect beam with pillars. This component combines thousands of independent members into intact structures, which are able to satisfy design requirements and bear a variety of external loads (Chun *et al*. 2011). Fig. 1 shows the typical construction of ancient timber structures. The tenon-mortise connection makes joint strong and flexible, and it has excellent anti-rotation ability and good energy dissipation capacity as well (Erdil *et al*. 2005. Gao *et al*. 2008. Xie *et al*. 2008). The tenon-mortise joint acts as the core area of the force transmission, the semirigid connection damage could cause the building to incline or even collapse, so it plays a significant role in ensuring the safety of wood structures. At the same time, the research on the mechanical properties of mortise-tenon joint is also the foundation of the repair and protection of ancient timber structures.

Xie *et al*. (2014) studied the rotational stiffness and energy dissipation capacity of damaged joints. Pang *et al*. (2010) evaluated the influence of beam shoulder on the moment-carrying capacity of traditional post-beam joints, dovetailed mortise, and tenon joints, and moment-carrying

(a) The whole structure

(b) Joint construction   (c) Bracket

Fig. 1 Typical timber structures

capacity was investigated by static loading tests. The results of the tests indicated that the moment resistance, joint stiffness, and failure modes were different with or without beam shoulder, the beam shoulder must be considered as an important factor in the structural design of traditional post-beam joints. A comprehensive study has been carried out on

∗Corresponding author, Professor
 E-mail: jianyang_xue@163.com

the flexural behaviour of dovetail mortise-tenon joints in timber structures by Chen *et al.* (2016), the results showed that the main failure mode of the dovetail joints is pull-out. The gaps within the joint have a great influence on the flexural behavior, and the side gaps have been found to affect more significantly than the top gaps, whereas the gaps on the apex have had the least effect. Chang (2006) studied the rotational performance of the traditional piercing connection in Taiwanese traditional style buildings, and obtained the relationship between the rotation stiffness and the rotation angle of the piercing connection. Chen (2011) researched the anti-rotation performance of the typical beam-column mortise-tenon joint of the Yingxian wooden tower through the low cyclic loading test, and established the refined finite element model of mortise-tenon joint. Yao *et al.* (2006) carried out the low cyclic loading test on typical mortise-tenon joints in historic timber buildings, by simulating the state of mortise-tenon joint with the varied stiffness element, the relation between the varied stiffness and the relative flexibility was founded. It was shown that the stiffness of the mortise-tenon joint changed nonlinearly from 0.3062 to 23.6054 kN/m with the change of load.

Most existing wooden structures have experienced several hundred years of natural erosion, and many of that have different degrees of damage, such as loosening of tenon joints, property deterioration of wood decay, tilting of roof trusses, distortion of brackets and so on. Among them, the looseness of mortise-tenon joints is a typical damage type. However, the theoretical analysis on the moment-rotation relationship of mortise-tenon joints with different degrees of looseness in ancient timber structures has not been reported. Currently, the research on mortise-tenon joints is mainly experimental and finite element analysis. The theoretical research falls far behind of the engineering application, which restricts the further development of mortise-tenon joints in the ancient timber structure.

In this paper, the mechanical analysis of the through-tenon joints was carried out, and the theoretical formulas of the moment-rotation angle of the mortise-tenon joints under different looseness were established, which was verified by experimental research.
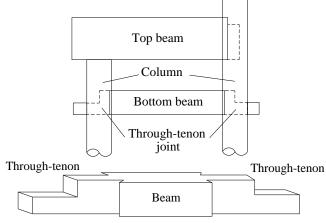
2. Mechanical behavior

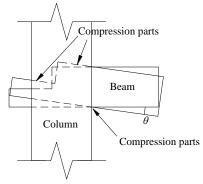Fig.2 Construction schematic diagram

2.1 Through-tenon joint configuration

Through-tenon is used in large timber construction, and often made into a small cross-section end shape, which is also known as the small-end tenon, as shown in Fig. 2.

Through-tenon is often installed between two pillars, which needs to be connected together. Neither can timber be welded, nor can bolts be used to connect it due to the unique properties of wood. Thus, holes need to be drilled in the timber columns to insert the beams and connect the structures. When the structure is subjected to extra external load, the through-tenon joint is able to bear certain bending moments and also produce certain rotation angle. It is a kind of semi-rigid connection method whose stiffness is between rigid connection and pin-hinged joints.
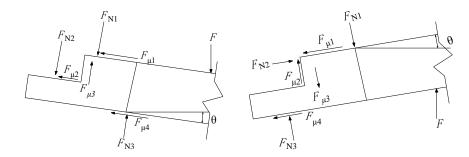
2.2 Force transmission

For the through-tenon joints with a certain degree of looseness, there is a gap between mortise and tenon. When subjected to the external load, the tenon produces slide firstly, and the friction of the mortise-tenon contact surface produces the rotational moment in the process of sliding. With the load increasing, a squeezing force occurred when the lateral sliding displacement is equal to the gap between the mortise and tenon, the tenon is under friction and compression together at that moment. Because the timber

(a) Sketch of tenon-mortise joint   (b) The stress diagram (positive loading)   (c) The stress diagram (negative loading)
Fig. 3 The mechanical analysis of mortise-tenon joint

elastic modulus along the grain is a lot bigger than that of the other directions, the embedding is more likely to occur on the beams.

As shown in Fig. 3(a), the tenon rotates around the outer edge of the mortise when the rotation angle θ is generated. The upper edge of the tenon is subjected to compressive stress on the upper surface of the mortise, and the lower intersection between pillar and tenon is under compression, that's to say, tenon end bears the force of F_{N1}, F_{N2} and F_{N3}. When the external load F increases gradually, the rotation angle θ increases as well. When the compression part of the wood entered into the plastic state due to compression perpendicular to the grain, resulting in the buried embedding effect, the mortise and tenon connect with each other more closely, then a certain force and bending moment are produced accordingly. During the rotation of the tenon, the resulting sliding makes the tenon end and the mortise surface produce friction $F_{\mu1}$, $F_{\mu2}$ and $F_{\mu4}$. As the loading continues, the embedding effect of the mortise-tenon joint becomes more obvious. The compressed tenon part is subjected to high-stress local extrusion, and the grain of this region becomes more dense owing to the buried embedding effect. In addition, through-tenon joints will not be destroyed from these parts generally from the experimental phenomenon.

When the rotation occurred between the tenon and mortise, tenon and mortise must have a certain slide, the longitudinal tension of the top edge of the tenon makes the emergence of the pull-tenon phenomenon, the pullout degree is generally low. However, due to the friction force $F_{\mu1}$ and buried embedding effect, it can restrain the continuous development of the pull-tenon phenomenon. At the same time, the tenon will be squeezed on the two sides parallel to the extrusion force. During the rotation process, a frictional force $F_{\mu3}$, which is parallel to the direction of the compression force, is generated on the contact surface between the mortise and the tenon. Briefly speaking, With the external force increasing, there will be pressure and friction force in this region, and the top edge moves outwards with respect to the pillar surface. Owing to the occurrence of friction, the longitudinal grain will elongate and a tensile force will appear on the top edge of tenon. In this way, the buried embedding effect, the friction force produced at the contact surface and the compression between mortise and tenon work together, and these forces are balanced with the moment produced by the external load.

3. Moment-rotation relationship

3.1 Basic assumption

The relative rotation between the parts of the mortise-tenon joint is mainly caused by the rotation of the tenon, and almost no shear deformation occurs in the panel zone. The failure phenomena mostly starts from the corner root of the tenon, and the shear distortion of the panel zone is neglected.

During the rotation of the tenon, a certain amount of pull out displacement is generated as a consequence of bending,

the external load bending point will change, but because the pulling force is relatively small, it can be considered that the external moment point is stable.

Based on the above analysis, the following basic assumptions can be made.

(1) The grain is along the longitudinal direction of column and beam. The timber is simplified as the orthotropic material. The constitutive law is assumed linear on the tension side and hardening bilinear on the compression side. In addition, tensile elastic modulus is equal to the compressive elastic modulus, and elastic stress - strain relationship conforms to Hooke's law.

(2) The shear deformation caused by the panel zone is not considered, only the rotation produced by the external load moment at the tenon end is taken into account.
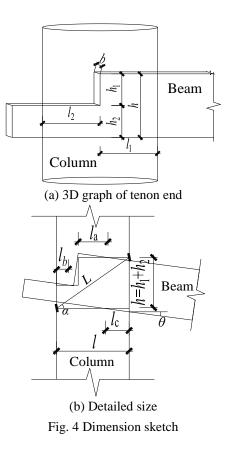
(3) The static and dynamic friction coefficient is equal and keep a constant value before and after the slide of mortise-tenon joint.

(4) It is assumed that the length of the external load arm is fixed during the rotation process of the tenon.

3.2 Formulas derivation

As shown in Fig. 3 and Fig. 4, when the mortise-tenon joint produces the rotation angle θ (including the rotation caused by the looseness), the tenon end is in the compression area. The rotation of the tenon end results in a certain degree of pull tenon, leading to a certain amount of extrusion and friction at the upper and lower surface of the tenon. The tenon extrusion deformation and dimensions are shown in Fig. 4.

According to the stress analysis and basic assumption of

(a) 3D graph of tenon end

(b) Detailed size

Fig. 4 Dimension sketch

the tenon, the bending moment of the through-tenon joints is mainly caused by three parts, including the moment caused by the buried embedding effect, the friction and squeezing force. In Fig. 3, $F_{\mu 1}$, $F_{\mu 2}$, $F_{\mu 3}$ and $F_{\mu 4}$ are the friction produced at the contact surface between the tenon and the mortise during the rotation of the tenon. F_{N1}, F_{N2}, and F_{N3} are the compressive forces of the through-tenon joint. From the mechanical analysis in Fig. 3 and equilibrium conditions, the following balance equation can be drawn when subjected to downward rotation, the deductive method of negative loading is the same.

$$\begin{cases} F_{N1} + F_{N2} + F\cos\theta = F_{N3} + F_{\mu 3} \\ F_{\mu 1} + F_{\mu 2} + F_{\mu 4} = F\sin\theta \end{cases} \quad (1)$$

According to the geometric relationship of Fig. 4, it is known as follows.

$$h_1 + h_2 + l_a \cdot \tan\theta + l_c \cdot \sin\theta \cdot \cos\theta = L \cdot \sin(\alpha + \theta) \quad (2)$$

Where h_1, h_2 are the cross-section height of the larger end and smaller end, respectively, l_a and l_c amount to the corresponding length of embedded region.

Morever, the rotation length $L = \sqrt{h^2 + l^2}$, which is the distance between the bottom left and upper right contact points between mortise and tenon, and rotation θ is the angle between this line and the horizontal, $\alpha = arc\tan(h/l)$, where $h = h_1 + h_2$, $l = l_1 + l_2$, l_1 and l_2 are the insertion length of larger end and smaller end in the mortise region, respectively.

The maximum strain along the embedding direction in the buried embedding region can be expressed as follows.

$$\begin{cases} \varepsilon_{\max,a} = \dfrac{l_a \sin\theta \cos\theta}{h/\cos\theta} = \dfrac{l_a \sin\theta \cos^2\theta}{h} \\ \varepsilon_{\max,b} = \dfrac{l_b \sin\theta \cos\theta}{h/\cos\theta} = \dfrac{l_b \sin\theta \cos^2\theta}{h} \\ \varepsilon_{\max,c} = \dfrac{l_c \sin\theta}{h} \end{cases} \quad (3)$$

Where $\varepsilon_{\max,a}$, $\varepsilon_{\max,b}$ and $\varepsilon_{\max,c}$ are the maximum strain value of larger end, smaller end and the bottom surface, respectively.

According to the assumption (1), the following equations can be obtained.

$$\begin{cases} \sigma_{\max,a} = \varepsilon_{\max,a} \cdot E_\perp \cdot \beta(\varphi) \\ \sigma_{\max,b} = \varepsilon_{\max,b} \cdot E_\perp \cdot \beta(\varphi) \\ \sigma_{\max,c} = \varepsilon_{\max,c} \cdot E_\perp \cdot \beta(\varphi) \end{cases} \quad (4)$$

Where $\sigma_{\max,a}$, $\sigma_{\max,b}$ and $\sigma_{\max,c}$ are the stress values corresponding to $\varepsilon_{\max,a}$, $\varepsilon_{\max,b}$ and $\varepsilon_{\max,c}$, respectively. $E_\perp$ is the transverse elastic modulus of wood (When the wood property enters into the compression plastic stage, the reduction coefficient of elastic modulus is considered as 0.3 (Xie *et al.* 2013)). The constitutive curve of the transverse compression of timber is shown in Fig. 5. $\beta(\varphi)$ is the magnification factor of wood elastic modulus, which is obtained by Hankinson Equation (Jozsef 1982).

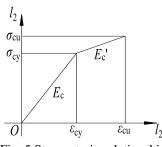$$\beta(\varphi) = \dfrac{E_{//}}{E_{//}\cos^n\varphi + E_\perp \sin^n\varphi} \quad (5)$$

Fig. 5 Stress-strain relationship

Where $E_{//}$ is the wood elastic modulus along the grain, n is the influence coefficient of different wood species, ranging from 1.5 to 2.0. As known from the literature (Ross 2010), n equals to 2.0. φ is the angle between the grain direction and the force direction. Moreover, $E_\perp(\varphi)$ equals to $E_\perp \cdot \beta(\varphi)$, which is the elastic modulus of wood at different force angles. The wood compression constitutive law adopts double-line hardening constitutive model according to the assumption (1), which is shown in Eq. (6).

$$\begin{cases} E_\perp(\varphi) = E_\perp \cdot \beta(\varphi) & \varepsilon \leq \varepsilon_y \\ E_\perp(\varphi) = E_{\perp,\tan} \cdot \beta(\varphi) & \varepsilon_y \leq \varepsilon \leq \varepsilon_u \end{cases} \quad (6)$$

Where: $E_{\perp \tan}$ is the elastic modulus when the wood entered into the hardening phrase, ε_y and ε_u are the yield strain and ultimate strain values, respectively.

The stress value $\sigma(\varphi)$ of the embedded region between the tenon and the mortise can be expressed by the Eq. (7).

$$\sigma(\varphi) = \begin{cases} E_\perp(\varphi) \cdot \varepsilon & \varepsilon \leq \varepsilon_y \\ E_\perp(\varphi) \cdot \varepsilon_y + E_{\perp,\tan} \cdot (\varepsilon - \varepsilon_y) & \varepsilon_y \leq \varepsilon \leq \varepsilon_u \end{cases} \quad (7)$$

According to the basic assumptions (1) and (3), combined with the formulas (4) and (7), the pressure of the tenon end can be obtained as following.

$$\begin{cases} F_{N1} = \dfrac{l_a \cdot b \cdot \varepsilon_{\max,a} \cdot E_\perp(\varphi)}{2} \\ F_{N2} = \dfrac{l_b \cdot b \cdot \varepsilon_{\max,b} \cdot E_\perp(\varphi)}{2} \\ F_{N3} = \dfrac{l_c \cdot b \cdot \varepsilon_{\max,c} \cdot E_\perp(\varphi)}{2} \end{cases} \quad (8)$$

When substituting Eq. (3) into Eq. (8), the below could be given.

$$\begin{cases} F_{N1} = \dfrac{l_a^2 \cdot b \cdot \sin\theta \cos^2\theta \cdot E_\perp(\varphi)}{2h} \\ F_{N2} = \dfrac{l_b^2 \cdot b \cdot \sin\theta \cos^2\theta \cdot E_\perp(\varphi)}{2h} \\ F_{N3} = \dfrac{l_c^2 \cdot b \cdot \sin\theta \cdot E_\perp(\varphi)}{2h} \end{cases} \quad (9)$$

In addition, the friction generated by the contact of the mortise-to-tenon joint is shown in Eq. (10).

$$\begin{cases} F_{\mu 1} = \mu \cdot F_{N1} \\ F_{\mu 2} = \mu \cdot F_{N2} \\ F_{\mu 4} = \mu \cdot F_{N3} \end{cases} \quad (10)$$

Where μ is the friction coefficient of wood.

During the tenon rotation process, there is squeezing action on both sides of the mortise, due to the through-tenon is not the same as the dovetail joint, which has the characteristics of narrow root and wide end, thus the extrusion pressure is relatively small, the resulting friction is small correspondingly. That is to say, the friction $F_{\mu 3}$ generated by extrusion effect can be ignored.

According to the construction method of through-tenon, the embedded length of l_a and l_b can be regarded as the same.

Uniting the above formula, combined with the basic assumptions, the following can be obtained.

$$\begin{cases} l_a = l_b = \dfrac{\kappa(l\sin(\alpha+\theta)-h)}{\cos^2\theta+\kappa} \\ l_c = \dfrac{l\sin(\alpha+\theta)-h-l_a^{\,2}}{\cos^2\theta} \end{cases} \quad (11)$$

Where $\kappa = \sqrt{\dfrac{(1-\mu)}{2\mu}}$. According to Eq. (11), the embedding length of the tenon is related to the friction coefficient μ, the cross-section height of the tenon h and the insertion depth of the tenon l. As the loosening degree of the tenon joints increases, the embedding insertion length of the tenon is reduced.

The following Eq. (12) can be obtained by solving the Eqs. (1), (8), (10) and (11).

$$F = \frac{b\mu\{l\sin(\alpha+\theta)-h-\{\frac{\kappa^2[l\sin(\alpha+\theta)-h]^2}{(\cos^2\theta+\kappa)^2}\}\}^2 \sin\theta(\cos\theta+\sin\theta)E_\perp(\varphi)}{(1+\mu)h\cos^4\theta}$$

$$(12)$$

To sum up, the relation of resistance moment M and the rotation angle θ is below.

$$M = Fs = \frac{b\mu s\{l\sin(\alpha+\theta)-h-\{\frac{\kappa^2[l\sin(\alpha+\theta)-h]^2}{(\cos^2\theta+\kappa)^2}\}\}^2 \sin\theta(\cos\theta+\sin\theta)E_\perp(\varphi)}{(1+\mu)h\cos^4\theta}$$

$$(13)$$

Where s represents the external loading arm.

Combined the previous research achievement (Zhang *et al.* 2013, Xie *et al.* 2014, Ogawa *et al.* 2016), the effect of different looseness of the tenon joints can be modified according to Eq. (14).

$$k = 1.189 - 2.977\theta \quad (14)$$

In conclusion, the expression between the moment M and the rotation angle θ of the through-tenon joints considering different looseness is as follows.

$$M = kFs = \frac{b\mu sk\{l\sin(\alpha+\theta)-h-\{\frac{\kappa^2[l\sin(\alpha+\theta)-h]^2}{(\cos^2\theta+\kappa)^2}\}\}^2 \sin\theta(\cos\theta+\sin\theta)E_\perp(\varphi)}{(1+\mu)h\cos^4\theta}$$

$$(15)$$

4. Experimental verification

In order to verify the rationality of the formula (15), the theoretical calculation results are compared with the experimental results by the pseudo-static test of through-
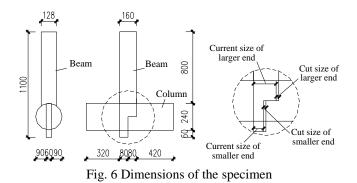

Fig. 6 Dimensions of the specimen

Table 1 The loosening degree of mortise-tenon joint

Specimen	Cut size of larger end /mm	Cut size of smaller end /mm	Current size of larger end /mm	Current size of smaller end /mm	Loosening degree
TJ1	0	0	160	80	—
TJ2	4	4	156	76	2.5%
TJ3	8	8	152	72	5.0%
TJ4	12	12	148	68	7.5%
TJ5	16	16	144	64	10.0%
TJ6	20	20	140	60	12.5%

tenon joints with different looseness (Xia 2015).

4.1 Specimen design and fabrication

In accordance with the "Examples of Engineering Application" of Qing dynasty, six through-tenon joints were fabricated with 1: 3.2 scale. Among those specimens, one is intact, and the remaining five specimens are not closely connected with varying loosening degrees. The model construction and details are shown in Fig. 6 and Table 1.

The mortise size of the loosening through-tenon joint is the same as that of the intact joint, and the cross-section height of tenon is reduced to simulate the looseness of the joint. The loosening degree D is defined as the ratio of the cut size to the initial section height. Fig. 6 shows the dimensions of specimens.

4.2 Loading scheme

The loading device is shown in Fig. 7, the column is disposed horizontally on the base, and it is fixed by the horizontal jack, which applies the lateral load at the column end. The beam is in vertical placement, the cyclic load is imposed by the MTS actuator and a spherical hinge connection is installed at the front end of the actuator which is connected with the beam.

The horizontal load is controlled by the displacement. At the beginning of the experiment, 10%, 20%, 30%, 40% and 50% of ultimate displacements are applied once, respectively, then the 60%, 80% and 100% of ultimate loading cycled three times until the tenon end fracture, which represents the damage of specimens (Li *et al.* 2016).

4.3 Material properties

The wood properties measured according to the Wood

(a) Sketch
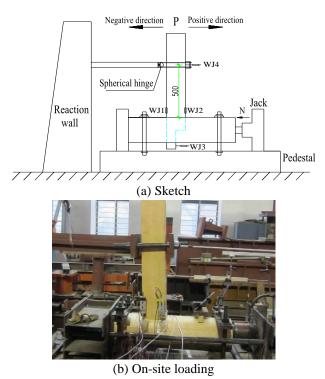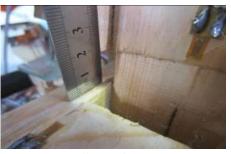

(b) On-site loading

Fig. 7 Test loading device

Table 2 Mechanical properties of the experimental wood

Tensile strength along the grain /MPa	Tensile strength across the grain /MPa	Compressive strength along the grain /MPa	Flexural strength /MPa	Moisture content %
54.3	3.2	23.2	35.9	13.3
Elastic modulus along the grain /MPa	Elastic modulus along the radial /MPa	Elastic modulus across the grain /MPa	Shear modulus /MPa	Shear modulus across the grain /MPa
10020	1150	530	268	154

(a) Pull-out of the tenon

(b) Tensile failure of the tenon-neck

Fig. 8 Failure modes of the mortise-tenon joints

Test Method are shown in Table 2. According to existing experimental study (Zhang 2013, Dong 2015), friction coefficient μ is taken as 0.45.

4.4 Test phenomena and failure modes

For the intact joint TJ1, after repeated extrusion loading, the mortise deformation was not obvious, a large number of plastic deformation occurred at the tenon. The wood fiber of tenon-neck cross-section was ruptured and extended to the tenon head obliquely, where bending failure appeared. The wood fiber was damaged along the grain at the transition tenon section in the negative loading direction, and the cracks extended to the root of the tenon.

For loosing joints (TJ2-TJ6), at the initial loading, free rotation occurred owing to different loosening degrees. As the load increases, the failure modes are similar to the intact one. The fracture location moved down from the tenon neck to the tenon head with the increase of loosening degrees. The detailed failure phenomena are shown in Fig. 8.

4.5 M-θ backbone curve

The backbone curve is the path connecting each cyclic peak point of the M-θ curve. The envelope curves of specimen TJ1-TJ6 from the experiment are shown in Fig. 9. The following conclusion can be drawn.

(1) For loosening through-tenon joints, there is a gap between the tenon and the mortise initially, and the bending moment increases slightly with the increase of the rotation angle. The slide section increases with the increase of the looseness of the joint at the first stage. In the later period of the loading, the loosening tenon joints turn to be compacted, and then the force status is similar to that of the intact joint.

(2) Comparing the backbone curves of each specimen, the ultimate moment of the loosening joint is less than that of the intact joint, while the ultimate rotation angle is greater than the intact one, and as the loosening degree increases, the limit bending moment decreases whereas the limit rotation angle increases.

(3) Due to the asymmetry of the through-tenon joint, the backbone curve is asymmetric correspondingly. Moreover, the ultimate rotation curve and ultimate bearing capacity of the reverse loading are less than those of the positive loading.
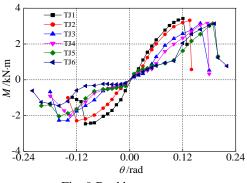

Fig. 9 Backbone curves

Table 3 The comparison analysis

Specimen	M_{ye} /kN·m	M_{yc} /kN·m	M_{yc} / M_{ye}	M_{ue} /kN·m	M_{uc} /kN·m	M_{uc} / M_{ue}
TJ1	2.41	2.54	1.05	2.94	3.02	1.03
TJ2	2.28	2.35	1.03	2.81	2.87	1.02
TJ3	1.72	1.62	0.94	2.71	2.65	0.98
TJ4	1.79	1.85	1.03	2.56	2.65	1.04
TJ5	1.91	1.84	0.96	2.60	2.45	0.94
TJ6	1.88	1.96	1.04	2.23	2.39	1.07

4.6 Equations validation

The comparison between theoretical calculation results and the test are shown in Table 3.

In Table 3, M_y and M_u represent yield moment and the ultimate moment, respectively. The subscripts "e" and "c" denote the experimental values and the calculated values, respectively. The average of M_{yc}/M_{ye} is 1.011, the standard deviation equals to 0.104, and variable coefficient amounts to 0.103. Those characteristic indices of M_{uc}/M_{ue} are 1.012, 0.099 and 0.098, respectively. The values of the characteristic points shown in the table are the mean values of positive and negative loads. It can be seen from Table 3 that although the calculation and experimental results are not all same, but they coincide quite well, which reflects the varing regulation of the moment and the rotation angle of the loosening through-tenon joints comprehensively.

5. Conclusions

(1) The M-θ backbone curve of through-tenon joints with different looseness shows that the ultimate moment of the loosening joint is less than that of the intact joint, while the ultimate rotation is greater than the intact joint, and the ultimate bending moment decreases and the ultimate rotation increases with the increase of looseness of the through-tenon joints.

(2) The rotational moment and the initial rotational stiffness of the through-tenon joints increase with the increase of the friction coefficient. The increase of the tenon section height can effectively improve the load bearing capacity of the through-tenon joints.

(3) The relationship between bending moment and rotation angle of through-tenon joints with different looseness is deduced. The theoretical calculation results agree well with the experimental results.

(4) The embedment length of the tenon increases with the increase of the friction coefficient of the wood and the insertion length of the tenon, while it decreases with the increase of the cross-section height of the tenon. The deduced theoretical formulas can provide the theoretical basis for the force analysis of the ancient timber buildings.

Acknowledgements

Reference

Chang, W. (2006), "Research on rotational performance of traditional Chuan-Dou timber joints in Taiwan", National ChenKung University, Tainan.

Chen, C., Qiu, H. and Lu, Y. (2016), "Flexural behaviour of timber dovetail mortise-tenon joints", *Constr. Build. Mater.*, **112**, 366-377.

Chen, Z. (2011), "Behaviour of typical joints and the structure of Yingxian Wood Pagoda", Harbin Institutive of Technology, Harbin.

Chun, Q., Yue, Z. and Pan, J. (2011), "Experimental study on seismic characteristics of typical mortise-tenon joints of Chinese southern traditional timber frame buildings", *Sci. China Technol. Sci.*, **54**(9), 2404-2411.

Dong, X. (2015), "Research on seismic behavior of Dou-Gong brackets used in ancient timber buildings under different Skew angle", Xi'an Univeristy of Architecture and Technology, Xi'an.

Erdil, Y., Kasal, A. and Eckelman, C. (2005), "Bending moment capacity of rectangular mortise and tenon furniture joints", *Forest Prod. J.*, **55**(12), 209-213.

Gao, D., Zhao, H. and Xue, J. (2008), "A seismic characteristics of bucket arch and mortise-tenon joint of ancient Chinese timber buildings: Experimental research", *J. Nat. Disast.*, **17**(2), 58-64.

Jozsef, B. (1982), *Mechanics of Wood and Wood Composites*, Van Nostrand Reinhold Compary, New York.

Li, Y., Cao, S. and Xue, J. (2016), "Analysis on mechanical behavior of dovetail mortise-tenon joints with looseness in traditional timber buildings", *Struct. Eng. Mech.*, **60**(5), 903-921.

Ogawa, K., Sasaki, Y. and Yamasaki, M. (2016), "Theoretical estimation of the mechanical performance of traditional mortise-tenon joint involving a gap", *J. Wood Sci.*, **62**(3), 242-250.

Pang, S., Oh, J., Park, J., Park, C. and Lee, J. (2010), "Moment-carrying capacity of dovetailed mortise and tenon joints with or without beam shoulder", *J. Struct. Eng.*, **137**(7), 785-789.

Ross, R.J. (2010), *Wood Handbook: Wood as an Engineering Material*, Press of the Pacific, Washington DC.

Xia, H. (2015), "Experimental study on seismic behavior of through-tenon joints under different degree of looseness in ancient wooden buildings", Xi'an University of Architecture and Technology, Xi'an.

Xie, Q., Cui, Y., Zhao, H. and Xue, J. (2013), "Study on calculation method of wood strength for ancient timber structure buildings", *J. Fuzhou Univ. (Nat. Sci. Ed.)*, **41**(4), 483-486.

Xie, Q., Du, B., Zhang, F., Zheng, P. and Xu, Q. (2014), "Theoretical analysis on moment-rotation relationship of dovetail joints for chinese ancient timber structure buildings", *Eng. Mech.*, **31**(12), 140-146.

Xie, Q., Zhao, H., Xue, J., Yao, K. and Sui, Y. (2008), "An experimental study on the strengthening of mortise-tenon joints in ancient Chinese wooden buildings", *Chin. Civil Eng. J.*, **41**(1), 28-34.

Xie, Q., Zheng, P., Xiang, W., Cui, Y. and Zhang, F. (2014), "Experimental study on seismic behavior of damaged straight

mortise- tenon joints of ancient timber buildings", *J. Build. Struct.*, **35**(11), 143-150.

Yao, K., Zhao, H. and Ge, H. (2006), "Experimental studies on the characteristic of mortise-tenon joint in historic timber buildings", *Eng. Mech.*, **23**(10), 168-173.

Zhang, F., Zhao, H., Xue, J., Xie, Q., Sui, Y. and Luo, Z. (2013), "Lateral load-resisting analysis and experimental verification of ancient timber column-frame based on swing-columns principle", *Indus. Constr.*, **43**(10), 56-60.

Zhang, X. (2013), "Dynamic analysis of ancient timber-frame buildings under seismic excitations", Xi'an University of Architecture and Technology, Xi'an.

CC

Nomenclature

$F_{\mu 1}$, $F_{\mu 2}$, $F_{\mu 3}$, $F_{\mu 4}$	Friction at the different contact surface between tenons and mortises
F_{N1}, F_{N2}, F_{N3}	Compressive forces at the different contact surface
F	External load
θ	Rotation angle of the beam
h_1, h_2	Cross-section height of the larger and smaller end, respectively
b	Width of the beam
h	Height of the beam
l_1, l_2	Insertion length of larger and smaller end in the mortise region, respectively
l	Width of the column
l_a, l_b, l_c	Embedded length of different mortise part
α	Angle index representing the ratio of beam height over column width
L	Rotation length
$\varepsilon_{\max,a}$, $\varepsilon_{\max,b}$, $\varepsilon_{\max,c}$	Maximum strain of larger end, smaller end and bottom surface, respectively
$\sigma_{\max,a}$, $\sigma_{\max,b}$, $\sigma_{\max,c}$	Maximum stress of larger end, smaller end and bottom surface, respectively
$E_\perp$	Transverse elastic modulus of wood
$E_{//}$	Wood elastic modulus along the grain
n	Influence coefficient of different wood species
$\beta(\varphi)$	Magnification factor of wood elastic modulus
φ	Angle between the grain direction and the force direction
$E_\perp(\varphi)$	Elastic modulus of wood at different force angles
$E_{\perp \tan}$	Elastic modulus when the wood entered into the hardening phrase
ε_y, ε_u	Yield strain and ultimate strain, respectively
$\sigma(\varphi)$	Stress at different force angles
μ	Friction coefficient of wood
M	Resistance moment
s	External loading arm
k	Correction factor
D	Loosening degree
Δ_u	Ultimate displacement
M_y, M_u	Yield moment and ultimate moment, respectively